Proceedings of Australasian Conference on Robotics and Automation, 2-4 Dec 2014, The University of Melbourne, Melbourne, Australia

Electronic training wheels: An automated cycling track stand

D. Wardle, T. Gregory, B. Cazzolato
University of Adelaide, Australia
daniel.wardle@student.adelaide.edu.au, thomas.gregory@student.adelaide.edu.au,
benjamin.cazzolato@adelaide.edu.au

Abstract

A track stand is the act of balancing a bicycle while stationary, an inherently hard technique to perform. Several devices exist that provide lateral stabilisation of a bicycle, though few are designed to assist a rider. In this paper the design and derivation of dynamics are detailed for a Single Gimbal Control Moment Gyroscope (SGCMG) retrofitted to an adult-sized bicycle. A linear control system is designed with corresponding simulations of the modelled system. Linear theory shows that a minimum rotor momentum is required for stabilisation. The physical system is described with results showing the rider track stand time has significantly increased with the SGCMG.

1 Introduction

Concepts to achieve or improve stability of vehicles have been around over a century. One of the first examples is a working prototype of a monorail developed by Louis Brennan [1905], which achieved balance through two gyroscope rotors. The idea has also been extended to other vehicles. For example, in 1912 Peter Schilovski produced plans for a two wheeled vehicle that would be balanced by a 40 inch diameter, 4.5 inch thick at the rim gyroscope rotor [Self, 2014]. While these concepts seek to achieve the same goal as this project, namely lateral stabilisation, the designs require modification for small-scale application. There are several designs specific to bicycles in the marketplace to assist in stability. The most widespread and simple method is training wheels. These are commonly used for children learning to ride and enable the rider to maintain balance while at slow speed and when stationary. Training wheels pose two problems for the device to be widely accepted for adult bicycles; the angle of tilt of the bicycle is heavily constrained which will effect performance of the bicycle turning, as well as this, training wheels are commonly associated with children so the public response of training wheels for adults would be poor. As a result, several more technical solutions have been created.

One of these more technical solutions is stabilisation through conservation of angular momentum, which has been utilised by a design produced by Gyrowheel. The concept involves a battery powered rotor in the front wheel of the bicycle [Clawson, 2014], through conservation of angular momentum (and resulting gyroscopic precession) the bicycle wheel will impede angular velocity about the roll or yaw axes. Active control and gyroscopic precession has been implemented on a design by Lam [2011], which employs a SGCMG mounted on a children's bicycle. The rotor spins at significant angular velocity and is rotated by the gimbal to exert a torque on the bicycle to keep the bicycle upright. The design is implemented on a children's bicycle and is designed for riderless operation. An alternative to gyroscopic precession is to directly apply a torque through a reaction wheel. A reaction wheel used to balance a bicycle is proven for use by Almujahed et al. [2009], where a rotor is rigidly attached to a motor which is fixed to the bicycle. When torque is applied by the motor it gives the rotor an angular acceleration and consequently a reaction torque is exerted on the bicycle. This design has been implemented on a low centre of gravity bicycle, which keeps moments due to gravity and the inertia low, reducing the required applied torque. Of the mentioned designs, a SGCMG similar to Lam [2011] was chosen to be retrofitted to the pannier rack of a bicycle.

The design of the SGCMG implemented in this paper was influenced by budget, the availability of the components, the operation volume, total mass and the performance. To conserve weight and increase inertia (and performance) the SGCMG rotor design has most mass on the outer radius. The materials available for manufacturing the rotor were aluminium and steel. Stainless steel was used because of its higher density and yield stress while being at a relatively low cost. A brushless DC motor directly drives the rotor, while being sup-

ported by the gimbal. The gimbal encloses the rotor which provides the rotor with an additional degree-of-freedom about the yaw axis. A brushless DC gearmotor drives the gimbal via a belt drive. The belt drive configuration is necessary because of the large length of the gearmotor. Aluminium is used for all the remaining parts to ensure low weight. A CAD rendered image of the SGCMG is presented in Figure 1.

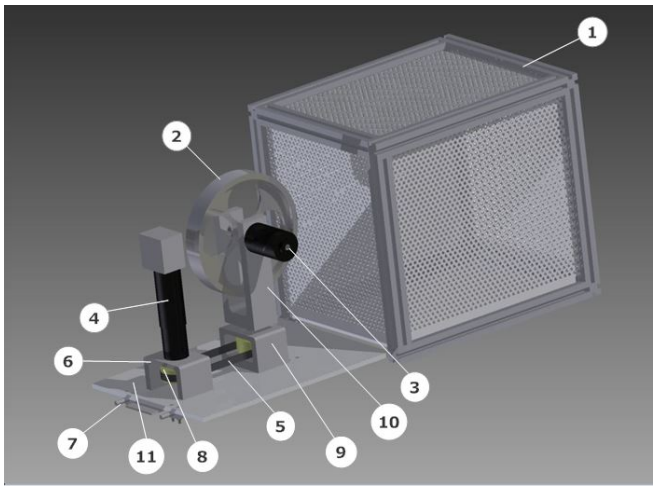

Figure 1: Rendered image of the SGCMG. 1) Safety Enclosure - When in operation the cage will be slid over to isolate the device from bystanders. 2) Rotor - Once up to speed, the angular momentum of the rotor is manipulated to produce a corrective torque. 3) Plettenberg Motor - The motor that drives the rotor. 4) Maxon Motor Assembly - Provides the torque that manipulates gimbal angle. 5) Timing Belt - Allows torque transmission from the Maxon Motor Assembly to the gimbal. 6) Maxon Motor Assembly Bracket - Holds the Maxon Motor Assembly and houses a timing pulley. 7) Bicycle Parcel Tray - This tray provides a base for components to be fixed to the bicycle. 8) Timing Pulley - In conjunction with the timing belt transmits torque. 9) Gimbal Bracket - Houses the gimbal axle and second timing pulley. 10) Gimbal - Houses the rotor and associated bearings. 11) Bottom Plate - Holds all sub-assemblies and connects to the bicycle parcel tray.

This paper details the dynamics and control of a bicycle with an attached SGCMG as part of an honours project conducted at The University of Adelaide. The dynamics of a generic stationary bicycle with an attached SGCMG are derived using the Lagrangian method. Parameters specific to the design that have been measured empirically or theoretically are provided. A preliminary control system for balance of a rigidly fixed human are presented with corresponding simulation results. The physical system is described with problems found during system integration. Results from the physical system with and without a rider on the bicycle are shown and discussed.

2 Modelling and Derivation of System Dynamics

A popular dynamic model to use for a bicycle is the Whipple model, which has a revolute joint for the steering, a revolute joint for each of the wheels to rotate and a revolute joint for roll of the bicycle. A similar model has been used by [Lam, 2011], where the only degree-of-freedom of the bicycle considered is roll. A similar model has been used in this paper for the derivation of the dynamics detailed below. The bicycle and attached components have a single degree-of-freedom about the roll axis and the SGCMG adds two more degrees-of-freedom for the gimbal and rotor rotation. In this model the human lean and front wheel rotation have not been included. These have been excluded due to the unpredictable nature that a human has on the control of the system.

In deriving of the system dynamics using the Lagrangian method, several simplifications and assumptions were made which are detailed below.

- The stationary components of the SGCMG (excluding the rotor and gimbal) were considered as a point mass at the combined centroid location.
- The steering of the bicycle was neglected in the modelling due to the unpredictable nature of different people balancing.
- The human was considered to be rigidly fixed to the bicycle, thus having the same angular rotation as the bicycle.
- The model consists of three revolute joints; the roll of the bicycle, rotation of the gimbal, and the rotation of the rotor.
- The y-axis of the bicycle and human is assumed to be a principal axis. The gimbal and rotor both have at least two principal axes such that the inertia tensor matrices are diagonal.
- The bicycle is assumed to be stationary longitudinally.
- Any losses from the belt drive are neglected.

To model the three degree-of-freedom system there are four right-handed coordinate frames. The subscripts r, 1, 2 and 3 are used for the reference frame, bicycle, gimbal and rotor respectively; the coordinate frame locations can be seen in Figure 2.

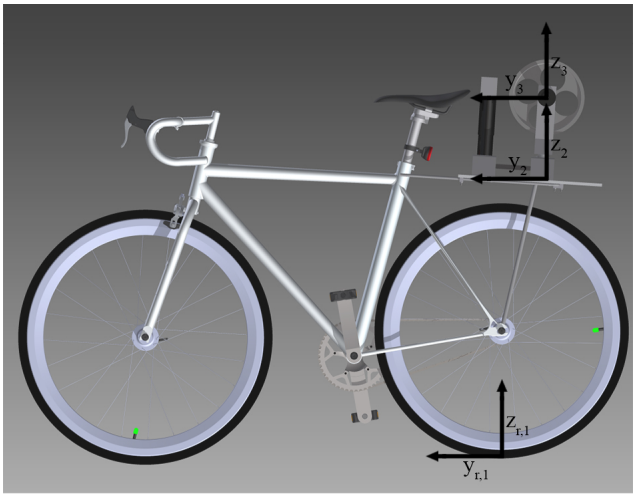

Figure 2: Diagram of locations of reference frames.

The model has three angular displacements which describe the three degree-of-freedom system:

- q_1, the roll of the bicycle which is the angular displacement about the y_1 axis
- q_2, the rotation of the gimbal which is the angular displacement about the z_2 axis
- q_3 the rotation of the rotor which is the angular displacement about the x_3 axis

The system has been broken down into five components, which are the bicycle, gimbal, rotor, stationary SGCMG parts and the human. The energy within each of these is determined separately and combined in the Lagrangian.

2.1 Interia

The inertia matrix for the bicycle is given by

$$\mathbf{I}_1 = \begin{bmatrix} I_{1xx} & 0 & I_{1xz} \\ 0 & I_{1yy} & 0 \\ I_{1zx} & 0 & I_{1zz} \end{bmatrix}.$$

The inertia matrix for the gimbal is

$$\mathbf{I}_2 = \begin{bmatrix} I_{2xx} & 0 & 0 \\ 0 & I_{2yy} & 0 \\ 0 & 0 & I_{2zz} \end{bmatrix}.$$

The inertia of the rotor is the same about two of the axes, therefore it has only two unique moments of inertia, represented as

$$\mathbf{I}_3 = \begin{bmatrix} I_{3xx} & 0 & 0 \\ 0 & I_{3yy} & 0 \\ 0 & 0 & I_{3yy} \end{bmatrix}.$$

The inertia of the human is

$$\mathbf{I}_5 = \begin{bmatrix} I_{5xx} & 0 & I_{5xz} \\ 0 & I_{5yy} & 0 \\ I_{5zx} & 0 & I_{5zz} \end{bmatrix}.$$

2.2 Rotation Matrix

The rotation matrix from the bicycle frame to the gimbal and rotor frames is

$$\mathbf{R} = \begin{bmatrix} \cos(q_2) & \sin(q_2) & 0 \\ -\sin(q_2) & \cos(q_2) & 0 \\ 0 & 0 & 1 \end{bmatrix}.$$

2.3 Velocities

The angular velocity of the bicycle and all rigidly attached components with respect to the fixed frame is

$$\boldsymbol{\omega}_1 = \begin{bmatrix} 0 \\ \dot{q}_1 \\ 0 \end{bmatrix}.$$

The angular velocity of the gimbal is

$$\boldsymbol{\omega}_2 = \begin{bmatrix} \dot{q}_1 \sin(q_2) \\ \dot{q}_1 \cos(q_2) \\ \dot{q}_2 \end{bmatrix}.$$

The angular velocity of the rotor is

$$\boldsymbol{\omega}_3 = \begin{bmatrix} \dot{q}_3 + \dot{q}_1 \sin(q_2) \\ \dot{q}_1 \cos(q_2) \\ \dot{q}_2 \end{bmatrix}.$$

The linear velocity of each of the components centre of mass due to the roll of the bicycle is

$$\mathbf{v}_i = \begin{bmatrix} 0 \\ \dot{q}_1 l_i \\ 0 \end{bmatrix},$$

where the index i is $1, 2, 3, 4, 5$ for the bicycle, gimbal, rotor, stationary SGCMG components and human, respectively.

2.4 Kinetic and Potential Energy

The kinetic energy of the bicycle is given by

$$\begin{aligned} E_{k1} &= \frac{1}{2}(w_1^T I_1 w_1 + v_1^T m_1 v_1) \\ &= \frac{m_1 \dot{q}_1^2 l_1^2}{2} + \frac{I_{1yy} \dot{q}_1^2}{2} \end{aligned} \tag{1}$$

The kinetic energy of the gimbal is

$$\begin{aligned} E_{k2} &= \frac{1}{2}(w_2^T I_2 w_2 + v_2^T m_2 v_2) \\ &= \frac{m_2 \dot{q}_1^2 l_2^2}{2} + \frac{I_{2yy} \dot{q}_1^2 \cos(q_2)^2}{2} \\ &+ \frac{I_{2xx} \dot{q}_1^2 \sin(q_2)^2}{2} + \frac{I_{2zz} \dot{q}_2^2}{2} \end{aligned} \tag{2}$$

The kinetic energy of the rotor is

$$\begin{aligned} E_{k3} &= \frac{1}{2}(w_3^T I_3 w_3 + v_3^T m_3 v_3) \\ &= \frac{I_{3yy}\,\dot{q}_2^2}{2} + \frac{I_{3xx}\,(\dot{q}_3 + \dot{q}_1\,\sin(q_2))^2}{2} \\ &+ \frac{\dot{q}_1^2\,l_3^2\,m_3}{2} + \frac{I_{3yy}\,\dot{q}_1^2\cos(q_2)^2}{2} \end{aligned} \tag{3}$$

The rotational inertia of the fixed SGCMG components is assumed to be negligible with respect to the inertia due to the parallel axis theorem. The resulting lumped kinetic energy of the fixed components is

$$\begin{aligned} E_{k4} &= \frac{1}{2}(v_4^T m_4 v_4) \\ &= \frac{\dot{q}_1^2\,l_4^2\,m_4}{2} \end{aligned} \tag{4}$$

The kinetic energy of the human is

$$\begin{aligned} E_{k5} &= \frac{1}{2}(w_5^T I_5 w_5 + v_5^T m_5 v_5) \\ &= \frac{m_5\,\dot{q}_1^2\,l_5^2}{2} + \frac{I_{5yy}\,\dot{q}_1^2}{2} \end{aligned} \tag{5}$$

The total kinetic energy in the system is

$$E_k = E_{k1} + E_{k2} + E_{k3} + E_{k4} + E_{k5}\,. \tag{6}$$

The potential energy for the whole system can be represented as

$$E_p = g\,\cos(q_3)(m_5 l_5 + m_4 l_4 + m_3 l_3 + m_2 l_2 + m_1 l_1)\,. \tag{7}$$

2.5 Lagrangian

The Lagrangian is the difference between the kinetic and potential energy of a system, that is,

$$L = E_k - E_p\,. \tag{8}$$

The equations of motion can be expressed through Lagrange's Equations as

$$\frac{d}{dt}\left(\frac{\delta L}{\delta \dot{q}_i}\right) - \frac{\delta L}{\delta q_i} = f_i\,, \tag{9}$$

where f_i are the non-conservative forces which are not included in the Lagrangian. The non-conservative force in this model is the applied torque provided by the motor driving the gimbal, τ_2. The losses due to other non-conservative forces have been neglected.

2.6 Linearised Dynamics

The non-linear dynamics have been derived and implemented in Simulink alongside a SimMechanics model created with the same specifications used for verification. Due to the length of the non-linear dynamic equations they are not presented here. Instead, only the linearised equations are provided. The equations have been linearised about the operating point $q_1 = \dot{q}_1 = q_2 = \dot{q}_2 = 0$. The angular velocity of the rotor, $\dot{q}_3$, is assumed to be constant to allow the gyroscopic coupling term to be in the linearised equations. The angular acceleration of the roll of the bicycle and attached components is

$$\ddot{q}_1 = \frac{\left(\sum_{i=1}^{5} g\,l_i\,m_i\,q_1\right) - I_{3xx}\,\dot{q}_2\,\dot{q}_3}{I_{1yy} + I_{2yy} + I_{3yy} + I_{5yy} + \sum_{n=1}^{5} m_n\,{l_n}^2}\,. \tag{10}$$

The angular acceleration of the gimbal is

$$\ddot{q}_2 = \frac{\tau_2 + I_{3xx}\,\dot{q}_1\,\dot{q}_3}{I_{3yy} + I_{2zz}}\,, \tag{11}$$

where τ_2 is the torque applied (by the gearmotor) to the gimbal.

The parameters used in modelling of the system are presented in Table 1.

Table 1: Values of the parameters used for modelling of the system.

Component	Parameter	Value
Bicycle	m_1	13.1 kg
	l_1	0.45 m
	I_{1yy}	1.90 kg m^2
Gimbal	m_2	0.878 kg
	l_2	0.880 m
	I_{2xx}	3.76e-3 kg m^2
	I_{2yy}	3.15e-3 kg m^2
	I_{2zz}	9.95e-4 kg m^2
Rotor	m_3	2.38 kg
	l_3	0.957 m
	I_{3xx}	2.08e-2 kg m^2
	I_{3yy}	1.06e-2 kg m^2
	$\dot{q}_3$	15,000 RPM
Stationary SGCMG	m_4	10.7 kg
	l_4	0.862 m
Human	m_5	75 kg
	l_5	1.15 m
	I_{5yy}	10 kg m^2

The poles of the linearised system dynamics are $s = 0, 0, +27.0i, -27.0i$ rad/s, therefore the linearised system is marginally stable. If gyroscopic precession is excluded (setting $\dot{q}_3 = 0$), the dynamics resemble that of an inverted pendulum. In the inverted pendulum model, the poles are $s = 0, 0, -2.87, +2.87$ rad/s, hence the presence of the gyroscope moves the real poles to the imaginary axis. For the system under investigation, the angular momentum of the rotor at which the system changes from unstable to marginally stable is 3.44kg m^2, or equivalently a rotor speed of $\dot{q}_3 = 1583$ RPM. The root locus

of the system with variable of rotor angular velocity, $\dot{q}_3$, can be seen in Figure 3.

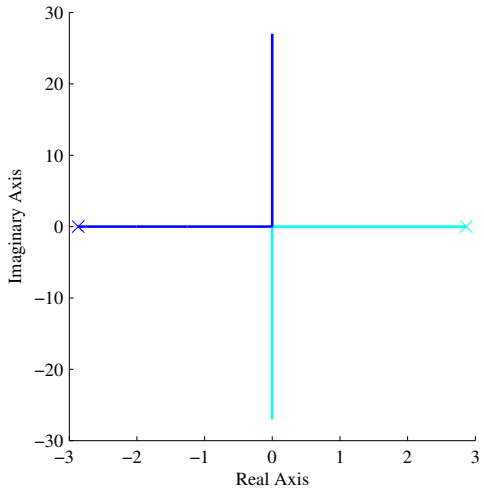

Figure 3: Root locus of linearised system dynamics for varying rotor angular velocity from 0 RPM to 15,000 RPM, where the poles become marginally stable at 1583 RPM.

The imaginary poles of the open loop linearised system with SGCMG at 15,000 RPM will produce a periodic response from the bicycle at a non-zero initial roll angle. The sinusoidal response is due to the kinetic energy being transferred between the SGCMG and the bicycle. When the bicycle falls it gives angular velocity to the gimbal through conservation of momentum. The periodic response of the system with the SGCMG at 15,000 RPM can be seen in Figure 4 along with the SGCMG response at 0 RPM.

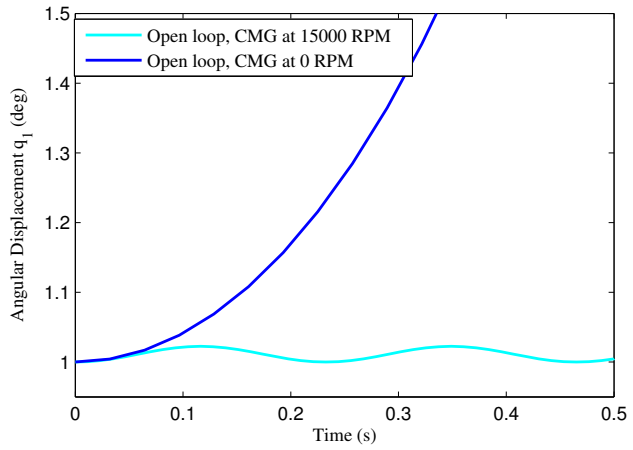

Figure 4: Open loop roll angle response of bicycle and SGCMG with rotor at 0 RPM and 15,000 RPM.

The system including the gyroscope has poles with no damping and the gyroscopic precession torque is always applied to the roll axis in the linearised model. Both of these lead to no energy being lost from the system. The non-linear model of the system includes the decreasing torque component acting about the roll axis of the bicycle. There is a sinusoidal relationship between the angle of the gimbal and the components of the gyroscopic torque in the roll and pitch axes of the bicycle (although pitch angle is assumed to be 0°). The difference between the non-linear and linear dynamics can be seen in Figure 5 by the difference in the roll of the bicycle, q_1, with an initial condition of $q_1 = 1°$.

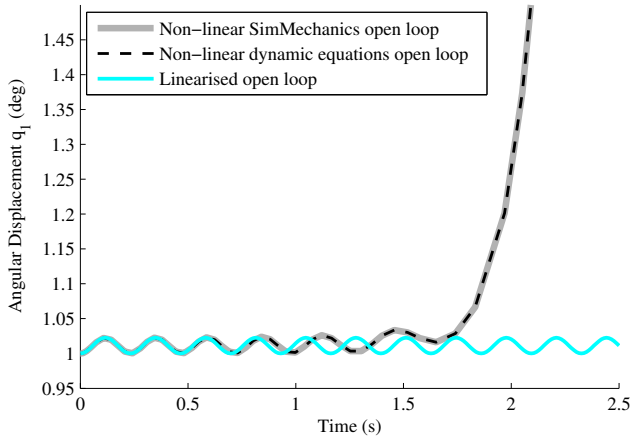

Figure 5: Linear and non-linear open loop response to initial condition of $q_1 = 1°$.

To maintain efficiency of the SGCMG, the control system should ensure that the gimbal angle, q_2, returns to approximately 0° when no assistance is required. That is, it is important that the average control moment should return to zero [Karnopp, 2002].

3 Control and Simulation

This section contains the preliminary control strategy implemented in simulation and the corresponding results. A Simulink model has been created from the non-linear equations to approximate the response of the real system to the control system. The dynamic equations have been verified through comparison with a SimMechanics model using the same specifications described in Section 2. A linear feedback controller has been used by Lam [2011], with linear feedback from the bicycle roll angle and angular velocity, as well as the angle of the gimbal. For the linear state feedback system presented in this section all four states are used for control of the system. The input into the system will be applied directly as torque on the gimbal, τ_2. To determine the control

gains a Linear Quadratic Regulator Method (LQR) was used.

To apply the LQR method, a state space model was constructed from Equation (10) and Equation (11). Following this, the weighting matrices $\mathbf{Q}$ and $\mathbf{R}$ were determined. As suggested by [Luo, 1995] the control weighting matrix, $\mathbf{R}$, is chosen to be a diagonal matrix whose values are $\frac{1}{(U_{imax})^2}$ where each U_{imax} is the maximum value of the control input. The $\mathbf{R}$ matrix was one dimensional due to the single input to the system. The influencing factor on the choice of this value is the maximum permissible torque of the gearmotor, which is 7.5 Nm. The $\mathbf{R}$ matrix was assigned to be

$$\mathbf{R} = \begin{bmatrix} \frac{1}{7.5^2} \end{bmatrix}. \tag{12}$$

The state weight matrix was found using the same approach as the control weighting matrix, that is, the diagonal entries were found by $\frac{1}{(X_{imax})^2}$ where X_{imax} is the maximum permissible value for the associated state. It was identified that there are two main states to be regulated for effective balance of the system, the gimbal angle q_2 and the bicycle roll angle q_1. Regulation of the bicycle roll angle is clear, while the gimbal angle should be minimised due to the cosine relationship between the gyroscopic precession torque acting on the roll axis of the bicycle and the gimbal angle. The state weighting matrix was chosen to be

$$\mathbf{Q} = \begin{bmatrix} 1000 & 0 & 0 & 0 \\ 0 & 0 & 0 & 0 \\ 0 & 0 & 10 & 0 \\ 0 & 0 & 0 & 0 \end{bmatrix}, \tag{13}$$

for a state vector of $\mathbf{x} = \begin{bmatrix} q_1 & \dot{q_1} & q_2 & \dot{q_2} \end{bmatrix}$. The control gains, $\mathbf{K}$, were found using the $\mathbf{Q}$ and $\mathbf{R}$ values stated using the LQR command in Matlab resulting in a control gain vector of

$$\mathbf{K} = \begin{bmatrix} -618 & -169 & -24 & 0.7 \end{bmatrix}. \tag{14}$$

The performance of the bicycle has been extensively simulated and the control gains were further adjusted to

$$\mathbf{K} = \begin{bmatrix} -620 & -215 & -7.5 & 2.45 \end{bmatrix}. \tag{15}$$

The implemented controller can be seen in the Simulink model in Figure 6.

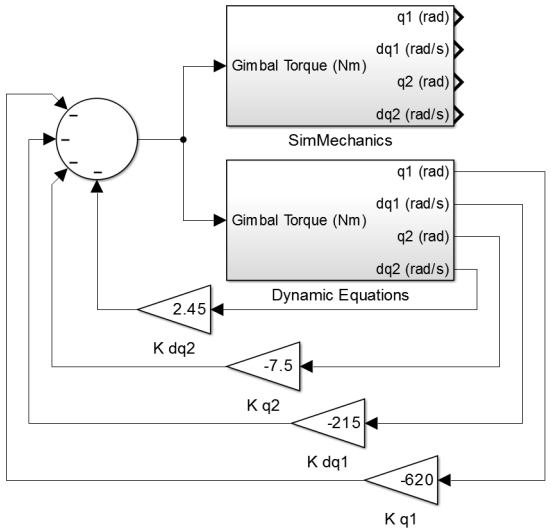

Figure 6: Simulink and SimMechanics models with control system.

To analyse the performance of the system the roll angle of the bicycle, q_1, was given a non-zero initial condition. From the initial condition, the response characteristics were observed, in-particular whether the system could be stabilised. Through trial and error it was determined that the maximum angle that the control system can stabilise the system is approximately 3.5°. The closed loop system response is shown in Figure 7.

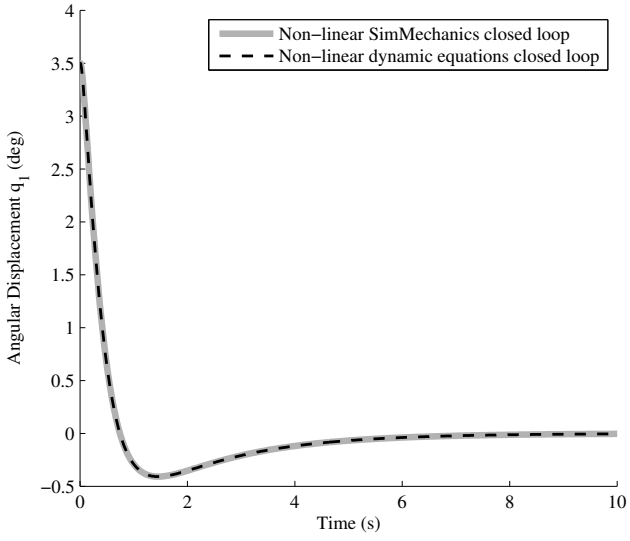

Figure 7: Closed loop response from initial condition $q_1 = 3.5°$.

4 Physical System

Construction of the physical prototype CMG has completed and is shown in Figure 8.

Figure 8: Bicycle with control moment gyroscope attached.

Initially a Microstrain FAS-A Inertial Measurement Unit (IMU) was used to sense the bicycle roll angle and angular velocity, however, this changed to a Microstrain 3DM-GX2 IMU for the final design. The rotor was driven by a Plettenberg 370/50/A1 S brushless DC motor which is controlled via a Castle Creations Phoenix Edge HV 160 speed controller. The rotor speed was measured through a tacho pulse provided by an auxiliary line from the Castle Creations speed controller. The gimbal is belt driven by a Maxon Motor 249000 gearmotor which is controlled by a Maxon Motor EPOS2 70-10 motor controller. The Maxon Motor 249000 gearmotor provides the gimbal position via an encoder and was initially controlled in current (equivalently torque) control mode but finalised to angular velocity control mode.

To provide system feedback to the rider a series of LED arrays were installed on the handlebars to indicate the rotor speed, IMU angle, and the gimbal position, which can be seen in Figure 9.

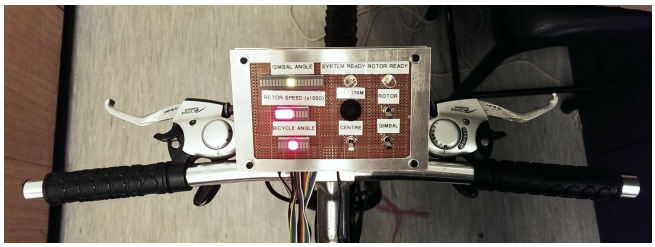

Figure 9: Peripherals for display of system values.

The LED arrays were driven via two microcontrollers. A Microchip dsPIC30F4011 was used to for interpretation of the gimbal position and bicycle roll angle, while an Arduino Mega 2560 was used for rotor speed.

5 Systems Integration

Whilst constructing the CMG and integrating this with the electrical equipment and the control systems, several major problems were found that hindered the stability of the bicycle.

5.1 Mechanical

During the initial stages of testing at 5,000 RPM the first attempts were unsuccessful. The system quickly went unstable after being activated. It was observed, that with the majority of the weight positioned over the bicycle's rear wheel that there was a mechanical resonance through the bicycle and the parcel tray of approximately 2Hz. With only thin aluminium rods connecting the bicycle's parcel tray to the frame, the tray could flex side to side easily at this resonance. To stiffen this link, a solid steel bracket was manufactured and attached in the same way. The bracket can be seen in Figure 10. With the inclusion of this bracket the effect of mechanical resonance feeding into the unstable gimbal lessened but the system was still unstable.

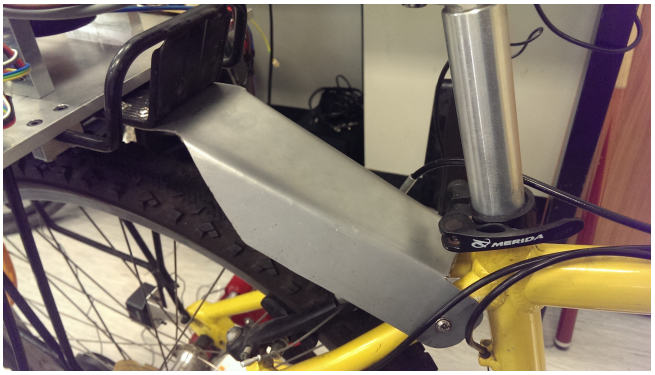

Figure 10: Bracket used to replace two aluminium slotted rods.

5.2 Electrical

The bracket had not changed the instability of the control system which led to investigation of the IMU. It was observed on the scope of the sensor signal there was significant noise. A significant control gain is applied to the derivative component of the roll angle, which when coupled with the noisy signal led created a large envelope for the steady state control signal. A single order 20Hz filter on the angle and a second order 20Hz filter on the velocity signal were implemented to attenuate some of the noise in the signal. The system became less volatile

as needed, however the system response was very slow, which prevented the system from being stable. After the FAS-A Microstrain unit was switched to the Microstrain 3DM-GX2, the control system was able to balance the bicycle in a riderless configuration on the first attempt. In Figure 11, the signals of the two different IMUs can be seen. The signal from the 3DM-GX2 is clearly less noisy which led to the stable system.

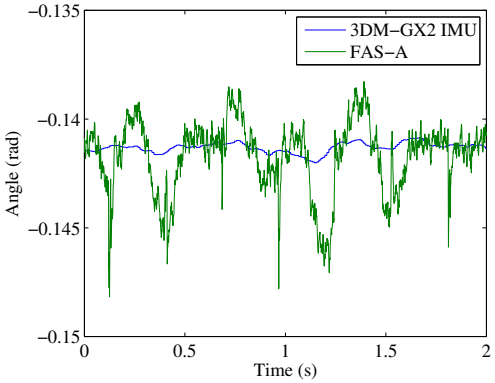

Figure 11: Comparison of the two IMUs.

5.3 Control

The current control system described in Section 3 was only implemented on the system without a rider. The control gains implemented for the bicycle are less than those found through simulation primarily due to the absence of the rider from the bicycle. The finalised current control gains were

$$\mathbf{K} = \begin{bmatrix} -350 & -50 & -10 & 2.45 \end{bmatrix}. \tag{16}$$

The current control system was able to balance the bicycle however due to stiction in the motor, the control signal needed to achieve a certain level before the gimbal could move from rest. This meant that the bicycle would fall for a small angle until the control signal was high enough for the gimbal to start moving. To improve the response and remove this lag in the system, the control system was changed to gimbal angular velocity control. This will apply as much current as is required for the gimbal to start movement and resulted in much smoother control with very little deviation from upright position once it had stabilised. The control gains for the velocity control mode used the same approach as Section 3. The final gains used on the system were

$$\mathbf{K} = \begin{bmatrix} -600 & -100 & -15 \end{bmatrix}, \tag{17}$$

for a state vector of $\mathbf{x} = \begin{bmatrix} q_1 & \dot{q_1} & q_2 \end{bmatrix}$.

6 Experimental Results

6.1 Riderless Testing

Initial testing of the stable system began in the riderless configuration. The rotor was spun to 10,000 RPM, the bicycle held approximately upright and the control system was then activated. The bicycle was quite stable as can be seen in Figure 12, where the bicycle angle and the gimbal angle are both displayed. The bicyle remains stable the entire time, even after two small disturbances were introduced by slightly pushing the bicycle sideways at approximately 7 and 12 seconds.

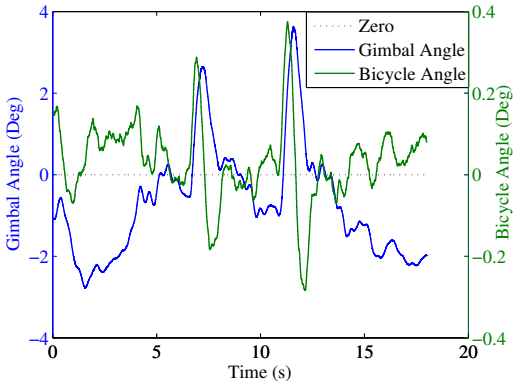

Figure 12: Riderless bicycle stabilisation at 10,000 RPM.

In Figure 12 it can be seen that whilst the bicycle is stable, that the angle of both the bicycle and gimbal drift away from zero. This is due to the IMU not reading exactly zero, bias was applied to the roll angle to ease this issue but it could not be eliminated completely. Once the gimbal has reached a small offset the control gain associated with the gimbal angle compensates for this effect.

6.2 Testing with Rider

After riderless testing was successfully completed, a rider was then introduced onto the bicycle. A regular 75 kg cyclist that did not possess the ability to track stand a regular bicycle was used as the tester in this stage.

Initially, the rider was instructed to rigidly attach themselves to the upright bicycle as best they could. The control system was then activated to investigate if a stable system was possible. This was considered unlikely as simulations suggested speeds approaching 15,000 RPM would be needed to balance a passive person of this size. Due to safety concerns, the system was only ever tested at a maximum speed of 10,000 RPM. This 'rigid body' testing comprised of three different tests: falling with no rotor speed, rotor at 10,000 RPM with no control and the rotor at 10,000 RPM with active control. The results are presented in Figure 13. It is shown that with

no control system active the gimbal can slow the fall of the rider by approximately half a second. What was more promising heading into track stand testing, was the system was able to correct the fall of the rider from an angle of 1.8 degrees before falling to the opposing side.

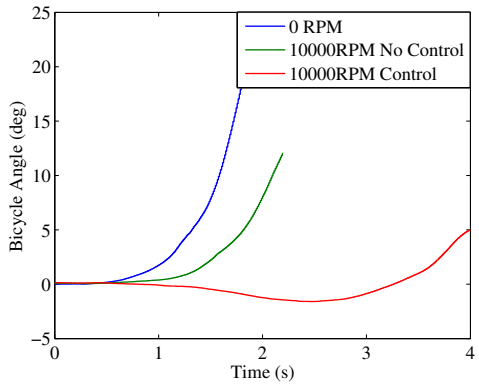

Figure 13: Comparison of 'rigid' body testing.

After rigid body testing, the rider moved into a regular track stand position which is shown in Figure 14.

Figure 14: Common track stand technique.

The rider was supported in the track stand position shown, the control system was then activated and the tester attempted to balance the bicycle upright for as long as possible. Figure 15 shows the results of one of these tests, where the bicycle's roll angle and the gimbal angles are both presented. After thirty minutes of testing time, the rider successfully kept the bicycle upright for more than 40 seconds (Figure 15). This is a good result considering the rider was unable to track stand more than 3 seconds with no aid from the CMG.

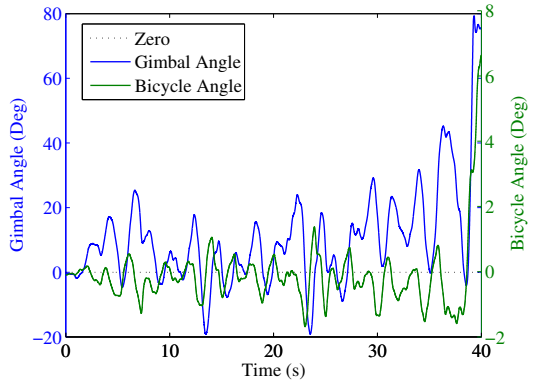

Figure 15: Tester track stand.

6.3 Results

As discussed in Sections 6.1 & 6.2, the testing phases provided several results. First of which was a stable system with no rider present at a rotor speed of 10,000 RPM. While not presented here, riderless stabilisation of the bicycle was also achieved at 5,000 RPM. Figure 13 shows that the CMG at 10,000 RPM was unable to stabilise the rider when they were 'rigidly' attached to the bicycle; however, the CMG was able to significantly delay the fall of the tester which gave confidence in the system moving forward. The final, and most significant, result was that, when in a track stand position, the tester was able to maintain balance for 40 seconds. The testing rider asserted that with little more practice that they believed this balancing time would increase quickly.

7 Conclusion

This paper details the derivation of the dynamics of the bicycle coupled with a SGCMG. It has been shown that the presence of the SGCMG changes the linearised dynamics from an inverted pendulum like model, to a marginally stable system when the rotor is above a minimum angular momentum. A controller developed with the LQR method is presented with corresponding simulations, showing the bicycle can be stabilised from an initial roll of 3.5°.

Testing of the system was completed with the method of control changing from current control to velocity control to decrease the non-linearity associated with the gearmotor driving the gimbal. After stability was achieved with the bicycle without a rider, a rider was introduced to the system which showed an increased stable time for the rider.

Acknowledgments

The authors would like to thank Mr Garry Clarke and all other contributing staff at the University of Adelaide Mechanical Workshop, and Mr Philip Schmidt and contributing staff from the University of Adelaide Electronic Workshop for manufacturing the required systems for the project. The authors would also like to thank LRD Engineering Pty Ltd for manufacturing key parts for the project.

References

[Almujahed *et al.*, 2009] Aamer Almujahed, Jason Deweese, Linh Duong, and Joel Potter. Auto-Balanced Robotic bicycle (ABRB). George Mason University, 2009.

[Brennan, 1905] Louis Brennan. Means for imparting stability to unstable bodies. US Patent 796893.

[Clawson, 2014] Trevor Clawson. Reinventing The (Gyro)Wheel – U.S. invented 'Cycling Toy' Reimagined In The UK. [Online - www.forbes.com/sites/trevorclawson/2014/04/28/reinventing-the-gyrowheel-us-invented-cycling-toy-reimagined-in-the-uk], accessed Nov. 2014.

[Karnopp, 2002] Dean Karnopp. Tilt Control for Gyro-Stabilized Two-Wheeled Vehicles. *Vehicle System Dynamics* , 37(2):145–156, 2002.

[Lam, 2011] Pom Y. Lam. Gyroscopic stabilization of a kid-size bicycle. *2011 IEEE 5th International Conference on Cybernetics and Intelligent Systems (CIS)* , pages 247–252, Qingdao, China, September 2011.

[Luo, 1995] Jia Luo and Edward C. Lan. Determination of weighting matrices of a linear quadratic regulator. *Journal of Guidance, Control, and Dynamics* ,18(6):1462–1463, 1995.

[Self, 2014] Douglas Self. The Schilovski Gyrocar. [Online - http://web.archive.org/web/20060703094337/http://www.dself.dsl.pipex.com/MUSEUM/museum.htm], accessed Nov. 2014.